PD IEC TR 61000-2-15:2023

BSI Standards Publication

Electromagnetic compatibility

Part 2-15: Description of the characteristics of networks with high penetration of power electronic converters

Documents
Document Sharing Hub

Full document details: PD IEC TR 61000-2-15:2023

National foreword

This Published Document is the UK implementation of IEC TR 61000-2-15:2023.

The UK participation in its preparation was entrusted to Technical Committee GEL/210, EMC - Policy committee.

A list of organizations represented on this committee can be obtained on request to its committee manager.

Contractual and legal considerations

This publication has been prepared in good faith, however no representation, warranty, assurance or undertaking (express or implied) is or will be made, and no responsibility or liability is or will be accepted by BSI in relation to the adequacy, accuracy, completeness or reasonableness of this publication. All and any such responsibility and liability is expressly disclaimed to the full extent permitted by the law.

This publication is provided as is, and is to be used at the recipient's own risk.

The recipient is advised to consider seeking professional guidance with respect to its use of this publication.

This publication is not intended to constitute a contract. Users are responsible for its correct application.

This publication is not to be regarded as a British Standard.

© The British Standards Institution 2023
Published by BSI Standards Limited 2023

ISBN 978 0 539 21316 4

ICS 29.240.01; 33.100.01

Compliance with a Published Document cannot confer immunity from legal obligations.

This Published Document was published under the authority of the Standards Policy and Strategy Committee on 31 March 2023.

Amendments/corrigenda issued since publication

Date	Text affected

Documents
Document Sharing Hub

Full document details: PD IEC TR 61000-2-15:2023

IEC TR 61000-2-15

Edition 1.0 2023-02

TECHNICAL REPORT

colour inside

Electromagnetic compatibility –
Part 2-15: Description of the characteristics of networks with high penetration of power electronic converters

INTERNATIONAL
ELECTROTECHNICAL
COMMISSION

ICS 29.240.01; 33.100.01

ISBN 978-2-8322-6550-5

Warning! Make sure that you obtained this publication from an authorized distributor.

® Registered trademark of the International Electrotechnical Commission

Documents
Document Sharing Hub

Full document details: PD IEC TR 61000-2-15:2023

CONTENTS

FOREWORD 8
INTRODUCTION 10
1 Scope 11
2 Normative references 11
3 Terms and definitions 11
4 Resonance phenomena with network and power electronics equipment based on actual cases 12
4.1 Operation of overvoltage protection of earth leakage circuit breaker in Japanese LV systems 12
4.1.1 General 12
4.1.2 Circuit modelling 13
4.1.3 Measurements on site 14
4.1.4 Technical or regulatory aspects 16
4.2 Analysis and modelling of an EV charging hub with PV production 17
4.3 Impact of power electronic household equipment on the impedance characteristics in residential networks 21
4.4 Harmonic resonance in an urban, residential low voltage grid 25
4.5 Harmonic distortion and impedance characteristics in an islanded microgrid 28
5 Impact of modern power electronics on the propagation and amplification of voltage distortion 31
5.1 Harmonic propagation in a residential LV network 31
5.1.1 General 31
5.1.2 Measurements 31
5.1.3 Modelling issues 33
5.2 Supraharmonic amplification in a residential LV network with a fast charging station 34
5.2.1 Measurement procedures 34
5.2.2 Measurement results 36
5.2.3 Simulation results 39
5.3 Supraharmonic amplification in a residential low voltage network with PV converters 41
5.4 Generic supraharmonic emission models for PWM based converters 42
5.5 Assessment of optimal impedance angles for power electronic devices to minimize risk of amplification 43
6 Cases of a large amount of converters 47
6.1 General 47
6.2 Large PV installations 48
6.3 Industrial grids 53
6.4 Multiple EV chargers in a central charging infrastructure 57
6.4.1 General 57
6.4.2 Measurements 58
6.4.3 Modelling of interactions between N similar single-phase power converters 59
7 Impact of grid conditions on the operation of converters 66
7.1 Analysis of a single-phase inverter model with an LCL filter using the Nyquist criterion 66
7.2 Probabilistic stability analysis for commercial low power inverters based on measured grid impedances 74

AVA Documents
Document Sharing Hub

7.3 Description of electric vehicles connected to a weak network ... 77
7.3.1 General ... 77
7.3.2 Modeling of the equipment involved ... 77
7.3.3 Determination of the voltage at the entrance of the charger, for different impedance values of the upstream network ... 79
7.3.4 Measurements performed at the manufacturer's laboratory ... 81
7.4 Other interactions between the grid and power converters ... 82
7.4.1 PV connected to a weak network ... 82
7.4.2 Windfarms connected to a grid ... 88
7.4.3 Microgrid during the islanding phase ... 89
7.4.4 Impact of the operating conditions ... 93
8 Harmonic emission characteristics of power electronic equipment for the mass-market ... 94
9 Conclusion and perspectives ... 97
9.1 General ... 97
9.2 Challenges ... 97
9.3 Main findings ... 98
9.4 Consequences ... 98
9.5 Recommendations ... 99
9.6 Future work ... 99
Bibliography ... 100

Figure 1 – Schematic illustration of a harmonic resonance issue in a LV system ... 12
Figure 2 – Waveform of the overvoltage at the neighbour side ... 13
Figure 3 – Description of an equivalent circuit modelling for harmonic resonances ... 13
Figure 4 – Electrical circuit used in simulations, and results of resonance magnification factors (RMFs) ... 14
Figure 5 – Description of the experimental test configuration ... 14
Figure 6 – Measurement performed during the experimental tests ... 15
Figure 7 – Resonance magnification factors (RMFs) using measurement and simulation ... 15
Figure 8 – Flowchart to assess an appliance's compliance with JIS TS C 0058 [2] ... 16
Figure 9 – Harmonic current limits for measurement assessment ... 17
Figure 10 – Trends of the number of inquiries regarding current emission limits in Japan ... 17
Figure 11 – Bloc scheme of the measured EV charging hub with PV production ... 18
Figure 12 – Power line impedance magnitude (top) and phase (bottom) measured at the point of common connecting (PCC) of an EV charger hub with PV production ... 19
Figure 13 – Resulting simplified model of the charging hub with distribution lines and feeder ... 19
Figure 14 – Impact of a super-fast EV charger on grid impedance ... 20
Figure 15 – Impedance characteristics of an urban LV network, ... 24
Figure 16 – Schema of the network ... 25
Figure 17 – Network harmonic impedance measured at different locations (L1-N) ... 26
Figure 18 – Simulated network harmonic impedance at different locations (L1-N) using default element representations ... 26
Figure 19 – Equivalent impedance model of a domestic customer ... 27

AVA Documents
Document Sharing Hub

Figure 20 – Measured and simulated network harmonic impedance at different locations (L1-N) using the developed customer impedance model 27
Figure 21 – Schematic representation of system under test 28
Figure 22 – Impedance characteristics (magnitude and phase angle) 29
Figure 23 – Voltage harmonic levels in ICM (a) and ISM (b) 30
Figure 24 – Simplified line diagram of the grid with marked measuring points 31
Figure 25 – Connection of a PQ measuring device 32
Figure 26 – Measured 15th current and voltage harmonic on phase L1 during operation of the heat pumps at the heat pumps' point of connection without active filter 32
Figure 27 – Measured voltage amplitudes of the 15th harmonic for each phase L1 to L3 during three different operating states without active filter 33
Figure 28 – Comparison of measured and simulated voltage levels (15th harmonic voltage) at each measuring point 33
Figure 29 – Modelled voltage vectors of the 15th harmonic at on- and off-state of the large heat pump without active filtering 34
Figure 30 – Spectrogram of the voltage at the point of injection of supraharmonic currents in a residential low voltage network 35
Figure 31 – Single-line diagram of relevant parts of the low voltage network 36
Figure 32 – Transfer ratio of supraharmonic voltage along the low voltage cable for phase L1 in case of single-phase injection at the transformer busbar BB 37
Figure 33 – Crosstalk ratio of supraharmonic voltage between phase L1 (phase of injection) and phase L2 at the junction box JB 38
Figure 34 – Measured impedance (magnitude and phase) of the DC charger in idle mode 38
Figure 35 – Transfer ratio along the cable for all three phases in case of three-phase injection at the transformer busbar BB 39
Figure 36 – Fully coupled three-phase simulation model 39
Figure 37 – Simplified simulation model for supraharmonic transmission along a low voltage cable 40
Figure 38 – Comparison of measured and simulated transfer ratios along a low voltage cable 40
Figure 39 – Transfer ratio of supraharmonic voltages along a low voltage cable of varying length 41
Figure 40 – Single-line diagram of the analysed low voltage network, two routes, and measurement locations on each route in red, green and blue 41
Figure 41 – Transfer ratios along two routes in a low voltage network with residential customers, upstream direction as circles, downstream direction as crosses 42
Figure 42 – Equivalent circuit (model) for the supraharmonic emission of single-phase voltage-source power converters for the mth emission band 43
Figure 43 – RMS voltage spectrum U_S at the output terminals of a single-phase power converter H-bridge using unipolar PWM 43
Figure 44 – Amplification and damping of supraharmonic emission at the POC relatively to the source voltage depending on the network to source impedance 45
Figure 45 – Circles of constant POC voltage in the dominant emission band of two photovoltaic inverters [29] 46
Figure 46 – Prevailing phase angle of 187 measured network loop impedances [34]between 2 kHz and 150 kHz, phase angle of the line impedance stabilization network from CISPR 16-1-2 46

Documents
Document Sharing Hub
Full document details: PD IEC TR 61000-2-15:2023

Figure 47 – Cumulative distribution function (CDF) of non-intentional emissions due to distributed energy sources at two different frequencies (45,7 kHz and 118,4 kHz) and noise present in the electrical grid (122,9 kHz) 47

Figure 48 – Identification of the frequencies in the frequency response 47

Figure 49 – Identification of the frequencies in the spectrogram of the measurements (see case study [23]) 48

Figure 50 – Parallel-connect configuration in large photovoltaic (PV) farm 49

Figure 51 – Simplified parallel of two converters featuring LCL filter and capacitor on common bus for reactive compensation in the grid (see Table 7) 49

Figure 52 – Frequency domain results of parallel LCL filter system with reactive power compensation capacitor represented in two frequency ranges 50

Figure 53 – N parallel connected equivalent inverter models equipped with LCL filter interfaces connected to common grid impedance $\boldsymbol{Z}_{\mathrm{g}}$ as parallel connection of Thévenin's equivalent voltage sources and equivalent impedances 51

Figure 54 – Change in Bode plot of $i_{\mathrm{sg}}/i_{\mathrm{s11}}$ (ratio of grid and inverter side currents respectively) or LCL-filter topology when the number of parallel connected inverters n increases from 2 to 8 with increments of 2 51

Figure 55 – Time domain simulations of parallel LCL system without reactive power compensation capacitor dependent on (in dependency of) a small sinusoidal disturbance term added in the control loop – Duty cycle 51

Figure 56 – Power line impedance in lower frequency range measured with 0 to 59 inverters activated in a 2,1 MW PV plant 52

Figure 57 – Power line impedance measured with 0 to 59 inverters activated in a 2,1 MW PV plant 53

Figure 58 – Configuration of an industrial grid 54

Figure 59 – Interaction between two converters, which can lead to resonances and generate non-intentional emissions in the 2 kHz to 150 kHz frequency range 54

Figure 60 – Modeling of a simple configuration of noise source and noise sink, where the EMI filter of the sink converter can be of 2nd, 3rd or 4th order [25] 55

Figure 61 – Impedance into the noise sink converter Z_{sink} with different EMI filter types with simple choke interface only and different EMI filter configurations 55

Figure 62 – Impedance into the noise sink converter Z_{sink} with different EMI filter types with LCL interface and different EMI filter configurations 56

Figure 63 – Ratio of voltage and current in phase 1 with a third-order EMI filter and different cables with: a) DM excitation and b) CM excitation 57

Figure 64 – Voltage at 10 kHz of one to four BEVs charging at a common POC, time varying values as solid line (20 ms measurement windows), overall RMS as dotted line 58

Figure 65 – Supraharmonic voltages and currents at the POC of multiple AC charging points, first emission band (800 Hz) centred around 10 kHz 59

Figure 66 – Single-line diagram of an arbitrary number N of power converters operating in parallel on a single network phase 60

Figure 67 – Supraharmonic emission model for an arbitrary number N of power converters operating in parallel 60

Figure 68 – Simulation of supraharmonic beating using summation of rotating phasors, for one up to three sources with different frequencies and magnitudes of contribution, first emission band 61

Figure 69 – Exemplary assessment of the supraharmonic emission of two photovoltaic inverters using the criteria in Formula (19) to Formula (21), and photovoltaic inverters from [15] 64

Documents
Document Sharing Hub

Full document details: PD IEC TR 61000-2-15:2023

Figure 70 – Dependency of the POC voltage on the number of sources N for different magnitude ratios of source impedance to network impedance assuming phase angles of source impedance and network impedance are equal 65
Figure 71 – Single phase inverter with an LCL filter and corresponding state variables 66
Figure 72 – Block scheme equivalent to the formula system of Figure 71 67
Figure 73 – Linearized control loop for the in-feed converter and transfer functions for feed forward and current measurement filter 68
Figure 74 – Norton equivalent circuit of the single-phase inverter 69
Figure 75 – Nyquist stability analysis of the control loop with parameters listed in Table 8 70
Figure 76 – PLECS model of the single-phase inverter with LCL filter 71
Figure 77 – PLECS model of the single-phase inverter controller with Feedforward of the connecting point voltage 71
Figure 78 – Simulation result of a current reference step of 0 A to 10 A for the converter 72
Figure 79 – Impedance magnitude (a) and phase angle characteristic (b) of commercially available single-phase inverter (black), network impedance with inductance of 2,3 mH (blue) and 3,2 mH (red) 73
Figure 80 – Grid-side current measurements for LR-equivalent network impedance with inductance values of 2,3 mH (a) and 3,2 mH (b) 74
Figure 81 – Small signal model of an inverter and the low voltage network 74
Figure 82 – Magnitude (a) and phase angle of low voltage network impedance measurements at 120 measurement sites 75
Figure 83 – Magnitude (a) and phase angle of the impedance of six commercially available inverters 75
Figure 84 – Critical frequency regions of commercially available inverters (a) and measurement sites in LV networks (b) 76
Figure 85 – Electrical network including the network and four electrical vehicles connected (described in the EMTP program) 77
Figure 86 – Description of the different elements considered 78
Figure 87 – Description of the filter connecting the boost to the electrical network 78
Figure 88 – Description of the low frequency filter 78
Figure 89 – Description of the converter of the boost PFC converter, including its AC/DC rectifier 79
Figure 90 – Current i_d flowing in the electronic components (diodes, IGBTs) versus positive values of the applied voltage V_d 79
Figure 91 – Voltage V_c at the entrance of the charger, obtained by simulations, for different values of the upstream network 80
Figure 92 – Description of the phase-space diagram corresponding to the main state-variables of the system 80
Figure 93 – Current crossing an IGBT obtained by simulations, with an inductance value of 600 μH for the upstream network 81
Figure 94 – Voltage V_{cmeas} at the entrance of the charger, measured at the manufacturer's laboratory, for a value of 750 μH for the inductance of the upstream network 81
Figure 95 – Description of the circuit including a solar PV–micro turbine based power system with battery backup 83
Figure 96 – PCC (grid) voltage with linear and non-linear loads in the absence of any VSI (voltage source inverter) 83
Figure 97 – Grid working and VSI switched on at t = 0,5 s 84

AVA Documents
Document Sharing Hub

Figure 98 – Grid working and VSI switched on at t = 0,5 s 85
Figure 99 – Frequency characteristic of the 3 kW PV system with L-C-L filter in the following grid conditions: A) 0,1 mH, B) 3 mH, C) 0,1 mH, 100 µF and D) 3 mH, 100 µF 85
Figure 100 – Resonance frequency variation in per cent of the rated resonance frequency as a function of grid inductance in per cent 86
Figure 101 – Illustration of a quasi-periodic route to chaos in a buck-boost converter, with the input voltage as a bifurcation parameter 87
Figure 102 – Experimental illustration of period doubling route to chaos in buck-boost converter 87
Figure 103 – Grid-connected DFIG WT system 88
Figure 104 – DFIG PQ limitation due to SCR and X/R variation 88
Figure 105 – System response to different network strength 89
Figure 106 – Structure of a hybrid system proposed for a microgrid application 90
Figure 107 – Control for a hybrid PV-battery system 90
Figure 108 – Variation of the voltage at the PV terminals and current in the battery 90
Figure 109 – Regulation of the voltage when the load is changing 91
Figure 110 – Current in the battery during variation of the voltage at the PV terminals during the change of load 91
Figure 111 – Microgrid system configuration and main features 92
Figure 112 – Designed PV microgrid system (left) and control set up of the PV microgrid at the Griffith University, Australia (right) 92
Figure 113 – Disturbance rejection response comparison in the intentional islanding scenario 93
Figure 114 – Description of a “test bench” at the laboratory 93
Figure 115 – Evolution of the measured current as a function of the charging setpoint 94
Figure 116 – Normalized input AC current waveforms of typical electronic appliances for sinusoidal (left) and flat-top (right) supply voltage waveforms 95
Figure 117 – Impact of voltage magnitude on harmonic current emission for different topology categories (sinusoidal waveform) 96
Figure 118 – Impact of flat top voltage waveform on harmonic current emission for different topology categories (nominal RMS voltage) 96

Table 1 – Relation between measured current and respective impedance for each feeder 21
Table 2 – Devices and topologies used in the different evolution stages 22
Table 3 – Load scenarios depending on the evolution stages and loading conditions 22
Table 4 – Equivalent $R_{L1}L_1||R_{L2}L_2C_2$ parameter values 23
Table 5 – Ratio between network harmonic impedance and extrapolated impedance for various cases 24
Table 6 – Load scenarios 29
Table 7 – Values of the system parameters [23] 49
Table 8 – Example of system parameters and components for the Nyquist stability analysis 71
Table 9 – Grid-compatibility index of commercially available single-phase inverters 76

Documents
Document Sharing Hub
Full document details: PD IEC TR 61000-2-15:2023

INTERNATIONAL ELECTROTECHNICAL COMMISSION

ELECTROMAGNETIC COMPATIBILITY –

Part 2-15: Description of the characteristics of networks with high penetration of power electronic converters

FOREWORD

1) The International Electrotechnical Commission (IEC) is a worldwide organization for standardization comprising all national electrotechnical committees (IEC National Committees). The object of IEC is to promote international co-operation on all questions concerning standardization in the electrical and electronic fields. To this end and in addition to other activities, IEC publishes International Standards, Technical Specifications, Technical Reports, Publicly Available Specifications (PAS) and Guides (hereafter referred to as "IEC Publication(s)"). Their preparation is entrusted to technical committees; any IEC National Committee interested in the subject dealt with may participate in this preparatory work. International, governmental and non-governmental organizations liaising with the IEC also participate in this preparation. IEC collaborates closely with the International Organization for Standardization (ISO) in accordance with conditions determined by agreement between the two organizations.
2) The formal decisions or agreements of IEC on technical matters express, as nearly as possible, an international consensus of opinion on the relevant subjects since each technical committee has representation from all interested IEC National Committees.
3) IEC Publications have the form of recommendations for international use and are accepted by IEC National Committees in that sense. While all reasonable efforts are made to ensure that the technical content of IEC Publications is accurate, IEC cannot be held responsible for the way in which they are used or for any misinterpretation by any end user.
4) In order to promote international uniformity, IEC National Committees undertake to apply IEC Publications transparently to the maximum extent possible in their national and regional publications. Any divergence between any IEC Publication and the corresponding national or regional publication shall be clearly indicated in the latter.
5) IEC itself does not provide any attestation of conformity. Independent certification bodies provide conformity assessment services and, in some areas, access to IEC marks of conformity. IEC is not responsible for any services carried out by independent certification bodies.
6) All users should ensure that they have the latest edition of this publication.
7) No liability shall attach to IEC or its directors, employees, servants or agents including individual experts and members of its technical committees and IEC National Committees for any personal injury, property damage or other damage of any nature whatsoever, whether direct or indirect, or for costs (including legal fees) and expenses arising out of the publication, use of, or reliance upon, this IEC Publication or any other IEC Publications.
8) Attention is drawn to the Normative references cited in this publication. Use of the referenced publications is indispensable for the correct application of this publication.
9) Attention is drawn to the possibility that some of the elements of this IEC Publication may be the subject of patent rights. IEC shall not be held responsible for identifying any or all such patent rights.

IEC TR 61000-2-15 has been prepared by subcommittee 77A: EMC – Low frequency phenomena, of IEC technical committee 77: Electromagnetic compatibility. It is a Technical Report.

The text of this Technical Report is based on the following documents:

Draft	Report on voting
77A/1153A/DTR	77A/1159/RVDTR

Full information on the voting for its approval can be found in the report on voting indicated in the above table.

The language used for the development of this Technical Report is English.

Documents
Document Sharing Hub

Full document details: PD IEC TR 61000-2-15:2023

This document was drafted in accordance with ISO/IEC Directives, Part 2, and developed in accordance with ISO/IEC Directives, Part 1 and ISO/IEC Directives, IEC Supplement, available at www.iec.ch/members_experts/refdocs. The main document types developed by IEC are described in greater detail at www.iec.ch/publications.

A list of all parts in the IEC 61000 series, published under the general title *Electromagnetic compatibility*, can be found on the IEC website.

The committee has decided that the contents of this document will remain unchanged until the stability date indicated on the IEC website under webstore.iec.ch in the data related to the specific document. At this date, the document will be

- reconfirmed,
- withdrawn,
- replaced by a revised edition, or
- amended.

IMPORTANT – The "colour inside" logo on the cover page of this document indicates that it contains colours which are considered to be useful for the correct understanding of its contents. Users should therefore print this document using a colour printer.

Documents
Document Sharing Hub

Full document details: PD IEC TR 61000-2-15:2023

INTRODUCTION

IEC 61000 is published in separate parts according to the following structure:

Part 1: General

General considerations (introduction, fundamental principles)

Definitions, terminology

Part 2: Environment

Description of the environment

Classification of the environment

Compatibility levels

Part 3: Limits

Emission limits

Immunity limits (insofar as these limits do not fall under the responsibility of the product committees)

Part 4: Testing and measurement techniques

Measurement techniques

Testing techniques

Part 5: Installation and mitigation guidelines

Installation guidelines

Mitigation methods and devices

Part 6: Generic standards

Part 9: Miscellaneous

Each part is further subdivided into several parts, published either as international standards or as technical specifications or technical reports, some of which have already been published as sections. Others will be published with the part number followed by a dash and a second number identifying the subdivision (example: IEC 61000-6-1).

This part of IEC 61000-2 describes the main phenomena which affect the power quality of modern distribution systems with high penetration of power electronics converters.

It focuses on the following main aspects: resonances in LV network, impact of increased number of power electronic converters, instability issues for the equipment to be connected to the LV networks.

Those new aspects, organized and described in this document, can lead to new IEC specifications; that is why a state of the art on this topic is necessary.

Documents
Document Sharing Hub

Full document details: PD IEC TR 61000-2-15:2023

ELECTROMAGNETIC COMPATIBILITY –

Part 2-15: Description of the characteristics of networks with high penetration of power electronic converters

1 Scope

This part of IEC 61000, which is a Technical Report, addresses in particular the following main phenomena, which affect the power quality in modern distribution systems with high penetration of power electronics converters. As some aspects of the subject have already been addressed in the past, considering the evolution of the LV and MV networks, this document focuses on the following aspects:

- resonances in the network, modelling and on-site validation;
- supraharmonics and measurements issues;
- impact of increased number of power electronic converters;
- stability and instability issues for the equipment to be connected

The target phenomena and conditions of this document are the following:

- frequency: ≤ 2 kHz, 2 kHz to 9 kHz, ≥ 9 kHz;
- voltage levels: LV, MV;
- harmonic sources: all types of converters (EV battery chargers, appliances, etc.…).

Some of these frequency ranges have already been standardized in some countries (Japan, Germany, Switzerland, etc.), but the resulting phenomena developed will benefit being described in more details, with a focus on the interaction between the converters and the electrical networks. The case of the presence of a large number of converters is also at stake. Some complex phenomena can also arise when the full system is not stable anymore.

NOTE Whereas it is expected that the models and derived calculations form this document can be applied to the Americas electrical systems its formal validation studies are still pending.

2 Normative references

There are no normative references in this document.

3 Terms and definitions

No terms and definitions are listed in this document.

ISO and IEC maintain terminology databases for use in standardization at the following addresses:

- IEC Electropedia: available at https://www.electropedia.org/
- ISO Online browsing platform: available at https://www.iso.org/obp

Documents
Document Sharing Hub

Full document details: PD IEC TR 61000-2-15:2023

4 Resonance phenomena with network and power electronics equipment based on actual cases

4.1 Operation of overvoltage protection of earth leakage circuit breaker in Japanese LV systems

4.1.1 General

- Overview

  In Japanese LV systems, power outages due to the operation of the earth leakage circuit breaker (ELCB) with an overvoltage protection function, and due to the abnormal acoustic noises generated by peripheral appliances can occur when particular appliances with power electronics technologies are operating [1][1].

  In some cases, the overvoltages exceed the rated voltage in the same LV system, caused by harmonics within the frequency band of 2 kHz to 9 kHz in the LV line.

  As a result of investigating these phenomena through verification tests and simulations, the overvoltage was confirmed as attributable to a harmonic resonance between the harmonic current produced by the power electronics appliance and the network circuit including the MV/LV transformer inductance, the LV line inductance and the-line capacitances with peripheral appliances. These resonance phenomena are also addressed in [7] [27].

  The case is addressed in detail in the following paragraphs, and other cases are mentioned in 4.2.

- Description of the conditions and their verification

  In Figure 1, when a particular power electronics appliance in a home (source) connected to a public LV system is in operation [1], an ELCB in another home (neighbour) connected to the same LV system acted and trips or acoustic noise from appliances occurred. The ELCB has functions not only to detect the earth leakage current but also to protect against overvoltages. That overvoltage protection operates when its amplitude exceeds 130 % of the nominal voltage.

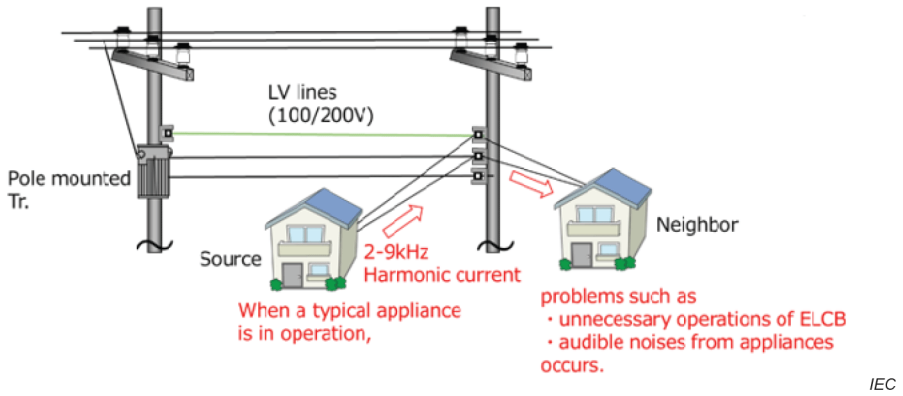

Figure 1 – Schematic illustration of a harmonic resonance issue in a LV system

The peak voltage in the waveform given by Figure 2 [1] exceeds 141 V_p of the normal peak voltage at 100 V_{rms} and includes harmonics in the higher frequency band. The overvoltage level at the neighbour location is higher than the one at the source because of a harmonic resonance.

[1] Numbers in square brackets refer to the Bibliography.

Documents
Document Sharing Hub
Full document details: PD IEC TR 61000-2-15:2023

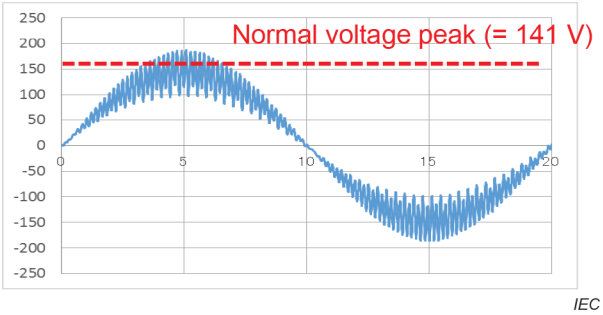

Figure 2 – Waveform of the overvoltage at the neighbour side

4.1.2 Circuit modelling

In Figure 3, the equivalent circuit of this parallel resonance consists of a harmonic current source I_n with a particular power electronics appliance, an MV/LV transformer inductance L_{tr}, an LV distributed line inductance L_{line}, a phase-to-phase capacitance C_0 connected to the appliance at the source side and a C_1 connected to appliances at the neighbour side. The voltage at the neighbor side is given by V_c as shown in Figure 2 [1]

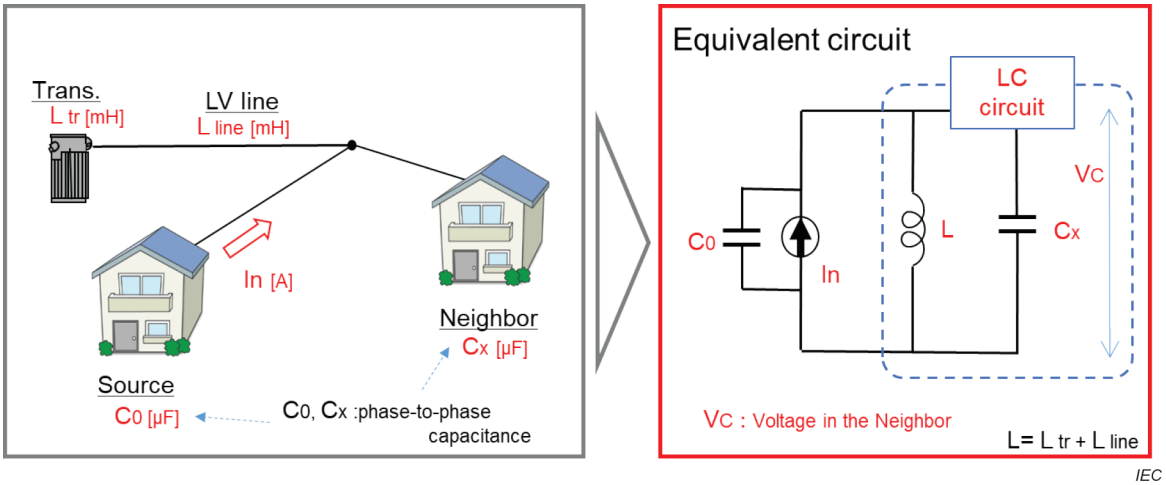

Figure 3 – Description of an equivalent circuit modelling for harmonic resonances

- Determination of the frequency dependent grid impedance (FdGI)

  From the equivalent circuit of an L, C parallel resonance, the resonance magnification factors (RMFs) (V/A) have been determined by simulations [1]. It can be seen in Figure 4 , using the frequency dependent impedance with the inductance of the LV system and the capacitor of the phase-to-phase capacitances with appliances.

  As the analytical parameters are in the frequency range from 2 kHz to 9 kHz, C_0 = 0,1∼1 000 μF and L_0 = 50 mH∼1 000 mH, are used on the source side with the power electronics appliance and C_1 = 1 μF∼2 0 μF is used on the neighbour side corresponding to the damaged equipment. The voltage when given by a current source of 1 A in the frequency band is defined as RMF.

Documents
Document Sharing Hub
Full document details: PD IEC TR 61000-2-15:2023

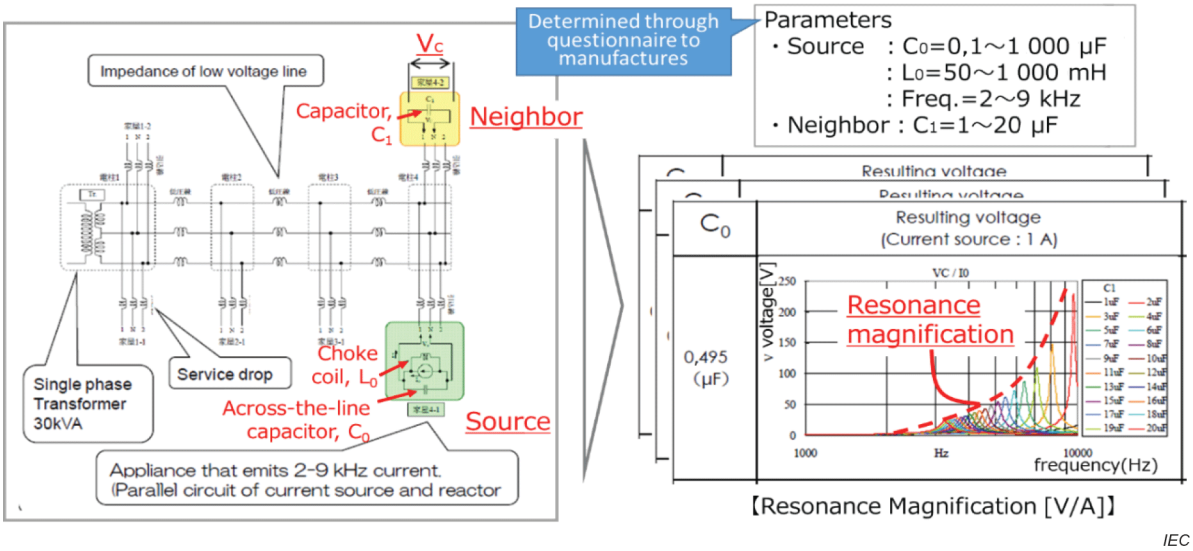

Figure 4 – Electrical circuit used in simulations, and results of resonance magnification factors (RMFs)

4.1.3 Measurements on site

The experimental tests which simulate the impedance of a typical LV system are performed in order to reproduce these resonance phenomena [1]. The capacitors at the connection point assumed for each household are connected to the emitted and the damaged devices, respectively, in Figure 5. In those tests, an appliance emitting harmonics at a terminal house and capacitors simulating the appliances of other houses are connected to the LV system. The voltages and currents at each connection point have been measured.

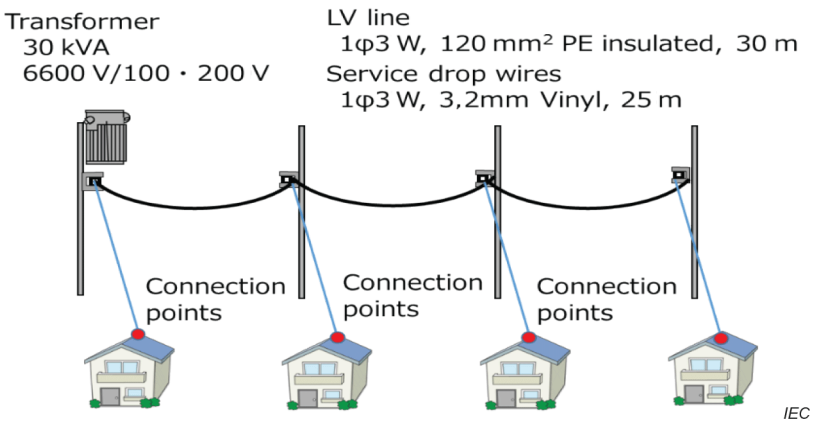

Figure 5 – Description of the experimental test configuration

As measured on site [1], a high-order harmonic voltage propagates to all the devices connected to the same system as the source. The resonance conditions depend on the impedance characteristics, so that the voltages are different depending on the measured location as shown in Figure 6:

Documents
Document Sharing Hub
Full document details: PD IEC TR 61000-2-15:2023

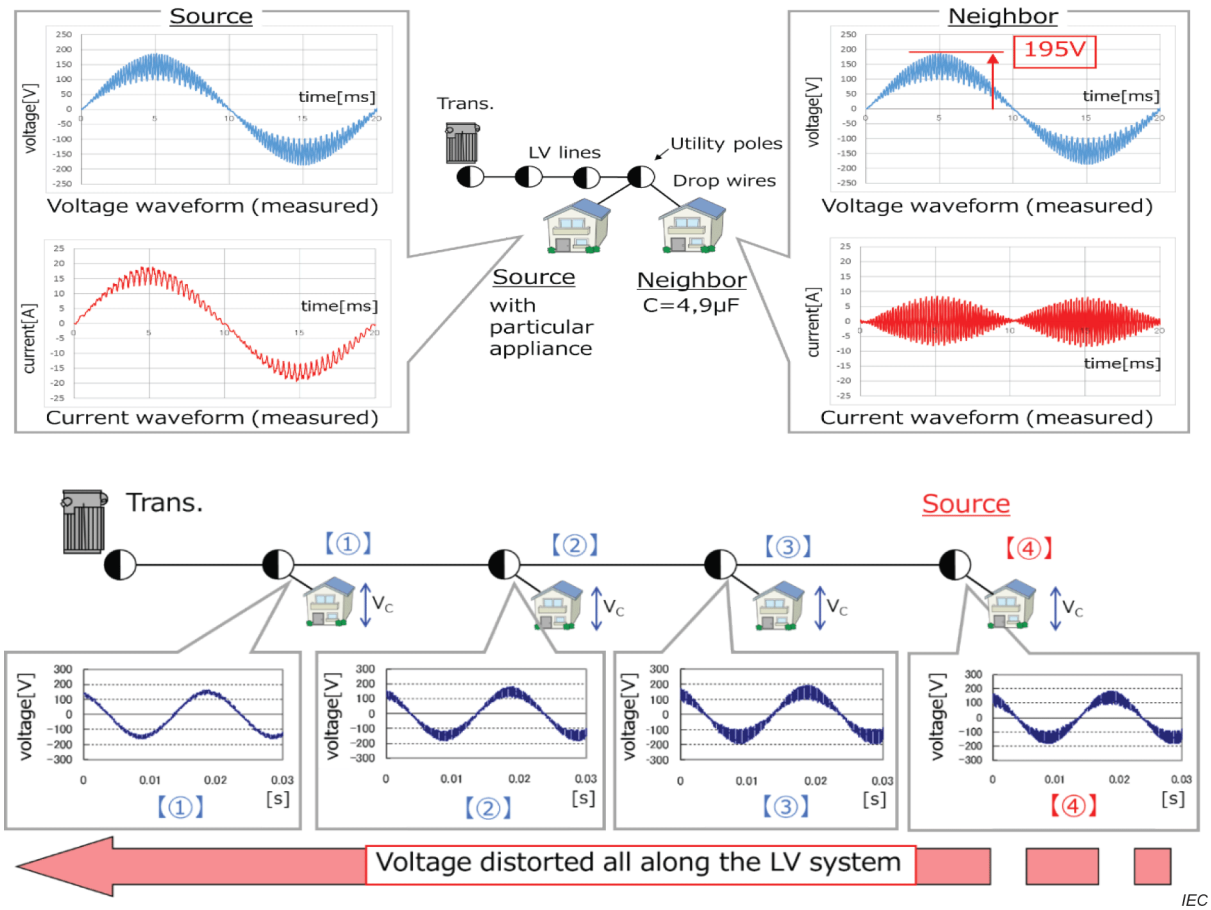

Figure 6 – Measurement performed during the experimental tests

In Figure 7, the voltage peak measured on site and the one obtained by simulation, under the same conditions, are in good agreement with a peak value equal to 65 V at 4,5 kHz [1].

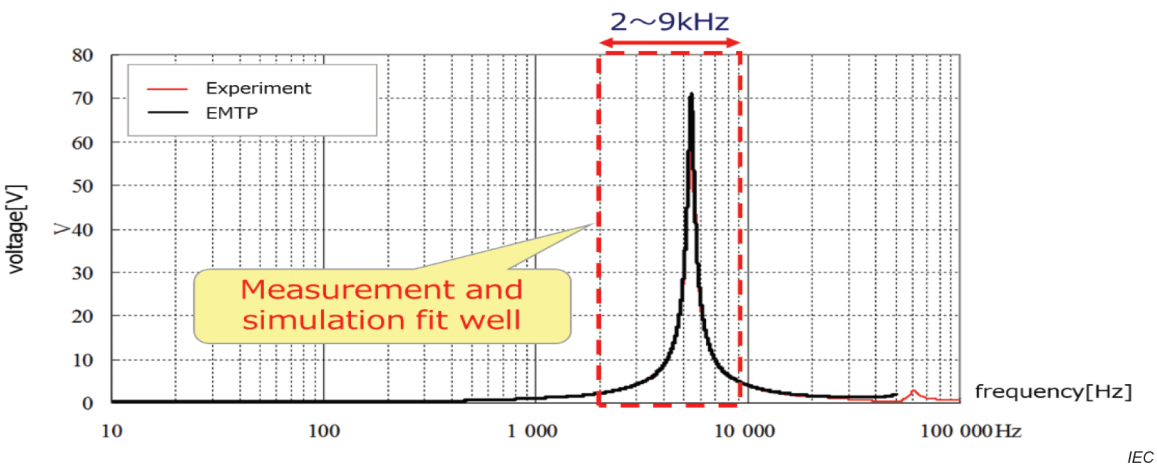

Figure 7 – Resonance magnification factors (RMFs) using measurement and simulation

The line resistances in the experimental LV system are considered as similar to those in the real LV system. However, the resistance loads contributing to the damping are not considered because there are many LV systems with almost no load.

Documents
Document Sharing Hub
Full document details: PD IEC TR 61000-2-15:2023

4.1.4 Technical or regulatory aspects

To establish countermeasures for these issues, the Japanese Industrial Standard on Technical Specifications JIS TS C 0058 [2] stipulates the emission limit values and assessment methods for harmonic currents in the range of 2 kHz to 9 kHz.

Reference [2] is intended to prevent the performance degradation and disturbances of other electric or electronic devices connected to public LV distribution system. The current emission limits of 2 kHz to 9 kHz are determined so that the voltage distortion does not exceed the immunity level of appliances. In addition, the overvoltage level is assumed by multiplying the harmonic current (A) by the resonance magnification factor (V/A).

The emission limits are calculated by using the capacity of the phase-to-phase capacitance built into the EUT (equipment under test) as a parameter. The measurement value would be lower than this limit value for each frequency of harmonics. The emission limit of the EUT that causes trouble is converted from “current value” to “power value” and can be assessed from the EUT design information (inverter control method, maximum input power, line capacitor capacity).

The flowchart in Figure 8 shows two types of assessments: “Design assessment” and “Measurement assessment” in order to reduce the cost for manufacturers. “Design assessment” is adopted so that the appliance complying with [2] can be assessed from the design information of the EUT to know in advance without measurements the switching frequency, the capacitance C_0 of the phase-to-phase capacitance with or without the interleaved mode. For instance, in the case where the switching frequency of the EUT is above 9 kHz or below 2 kHz, the EUT complies with [2] at the “Design assessment” stage.

Even if it does not satisfy the “Design assessment” conditions, the EUT complies [2] provided the measurement results satisfy the harmonic current limits in Figure 9 [2]:

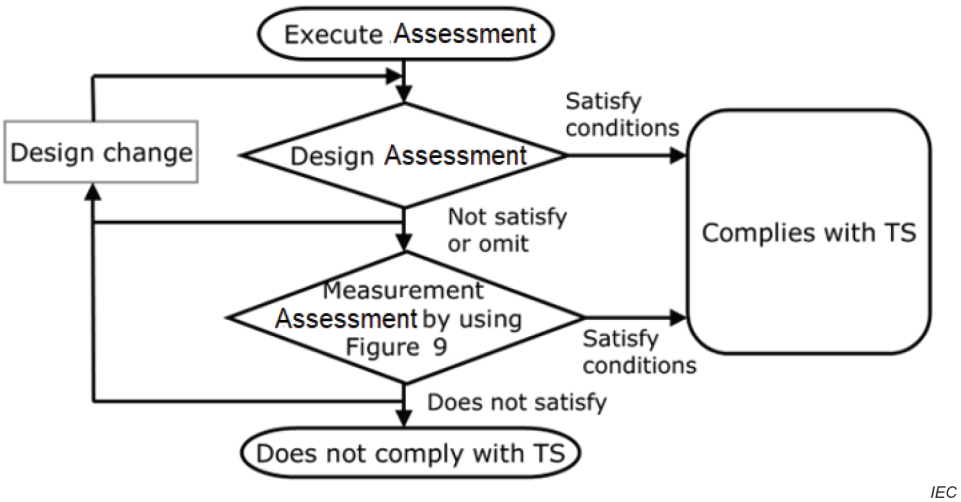

Figure 8 – Flowchart to assess an appliance’s compliance with JIS TS C 0058 [2]

Documents
Document Sharing Hub
Full document details: PD IEC TR 61000-2-15:2023

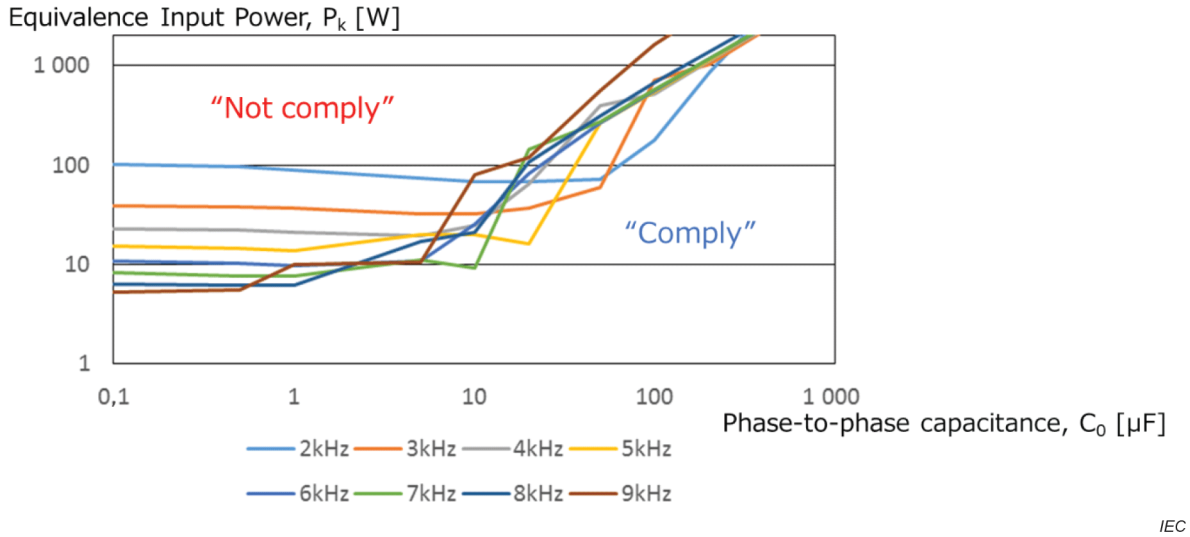

Figure 9 – Harmonic current limits for measurement assessment

- Impact on the equipment

  Reference [2] which stipulates the current emission limits in the range of 2 kHz to 9 kHz, is significant not only for sustaining the power quality for ten Japanese DSOs ("distribution system operators"), but also for producing the power electronics appliances for manufacturers [1]. The number of inquiries to DSOs regarding this issue decreased year after year thanks to the effort on [2] as shown in Figure 10. The appliance, which has harmonic current sources of 2 kHz to 9 kHz, was improved by the manufacturers before publishing reference [2].

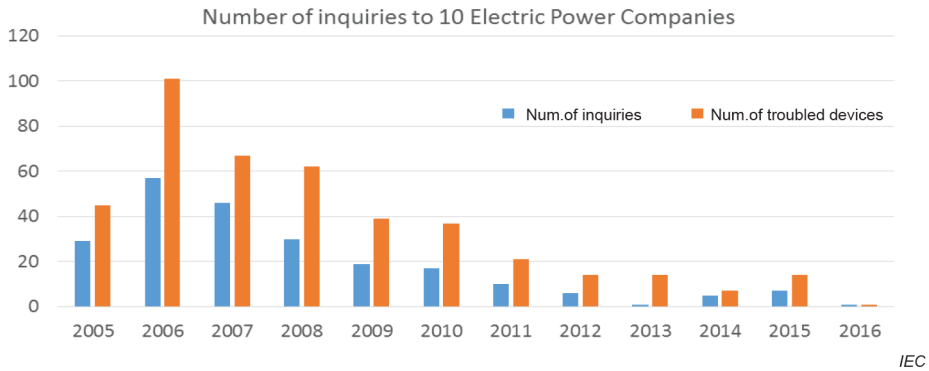

Figure 10 – Trends of the number of inquiries regarding current emission limits in Japan

Finally, these japanese technical specifications have been upgraded to a JIS Standard in 2020 [3].

4.2 Analysis and modelling of an EV charging hub with PV production

A measurement campaign has been carried out in a commercial building with an EV charging infrastructure and photovoltaic installations [4] (see Figure 11). High current peaks of up to 1,3 A on the 8th harmonic were measured at the fast charging stations during the transmission of ripple control signals transmitted at a frequency of 396 Hz. Although there were no problems with the transmission of the ripple control signal in this case, the parallel connection of several charging stations can affect communication. A high current due to a voltage harmonic generated by another converter at a resonance frequency could also damage the EMC filter capacitors at the input of one EV charger. This kind of effects can be considered when planning large EV charging hubs.

AVA Documents
Document Sharing Hub
Full document details: PD IEC TR 61000-2-15:2023

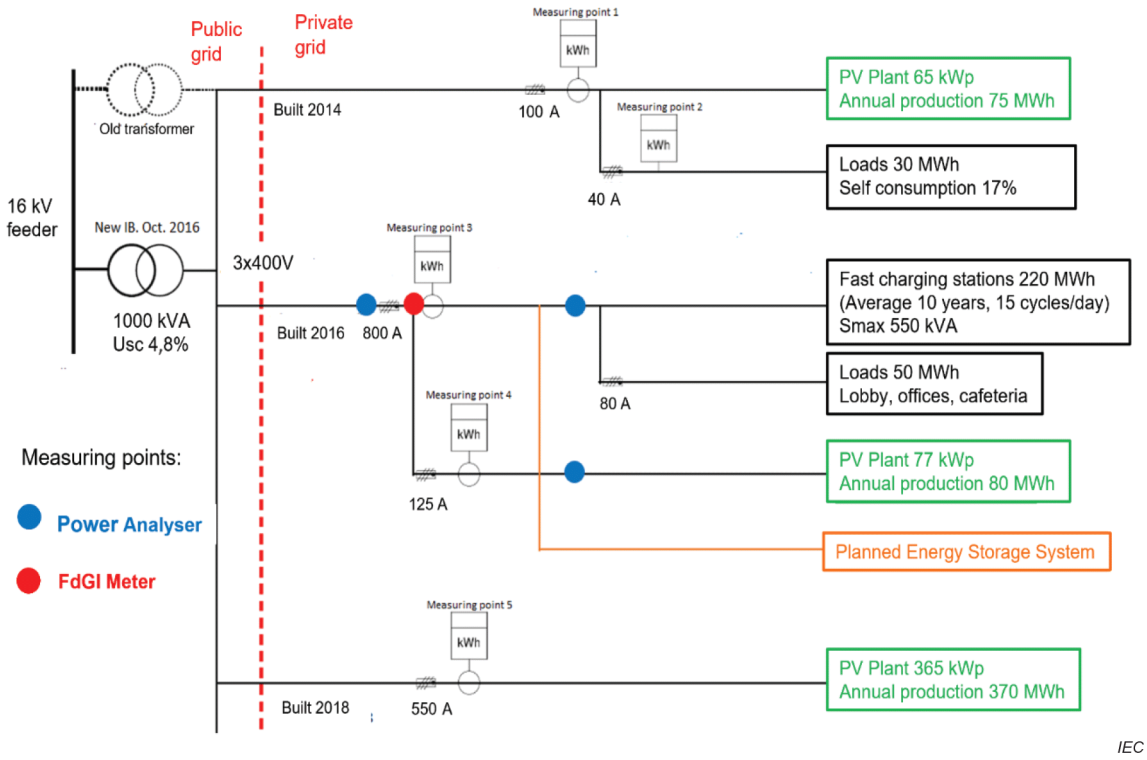

Figure 11 – Bloc scheme of the measured EV charging hub with PV production

These reflections motivated the modelling and the analysis of the situation with parallel connection of several converters with different types. The frequency-dependent grid impedance (FdGI) was in the frequency range between 150 Hz and 500 Hz, and was first measured on the busbar of the main distribution board of the installation as well as on individual feeders to different consumers, see Figure 12. The impact of FdGI was considered in both frequency ranges, below 2,5 kHz and above 2,5 kHz. A simplified electrical model of the system could be created based on the measured FdGI profiles (see Figure 13). The whole system with distribution to the 50 kW and 110 kW fast charging stations, to 22 kW charging stations for on-board chargers, and to the PV inverters showed a behaviour of the impedance, which was almost independent of the connected loads.

Documents
Document Sharing Hub
Full document details: PD IEC TR 61000-2-15:2023

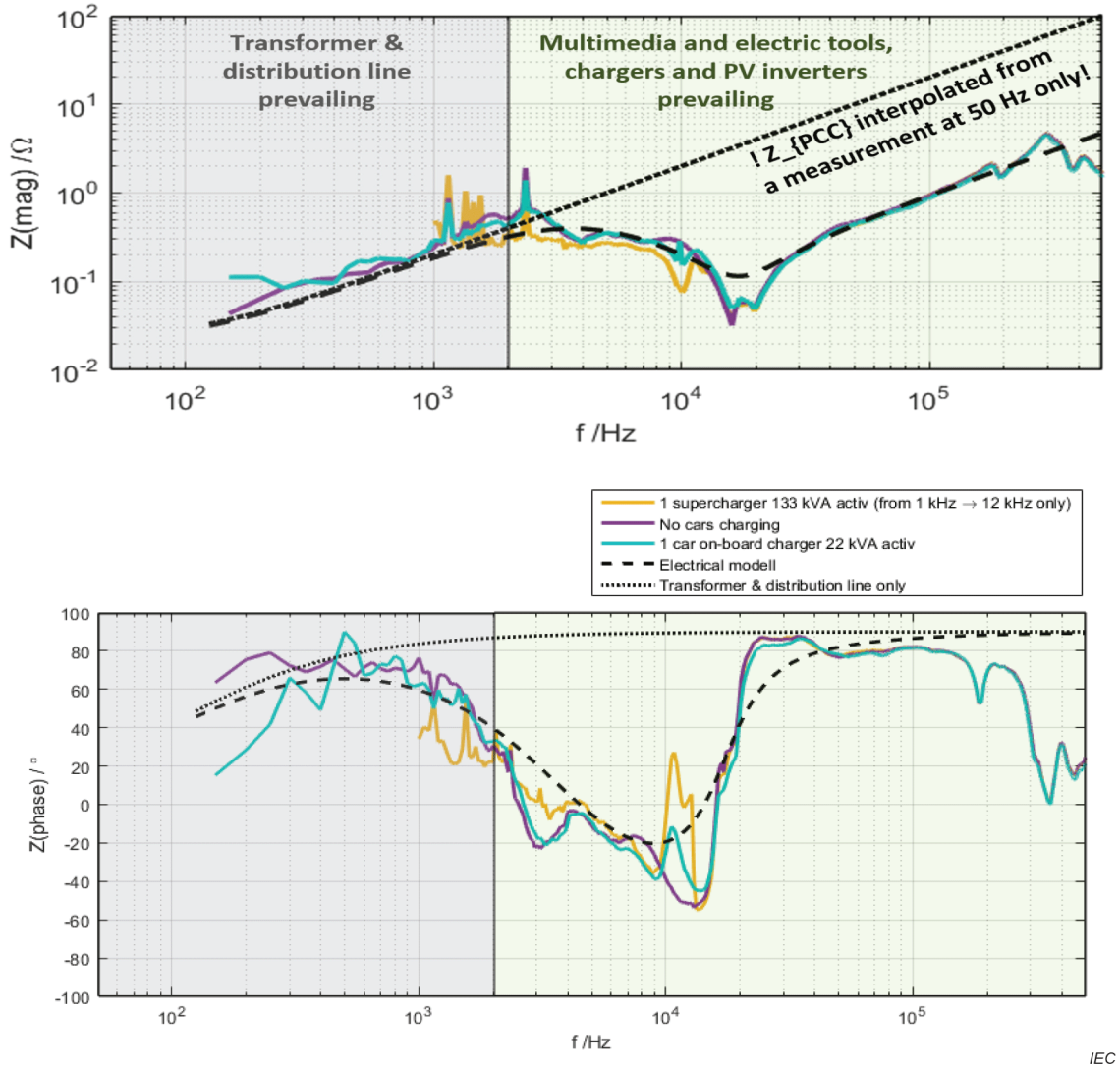

Figure 12 – Power line impedance magnitude (top) and phase (bottom) measured at the point of common connecting (PCC) of an EV charger hub with PV production

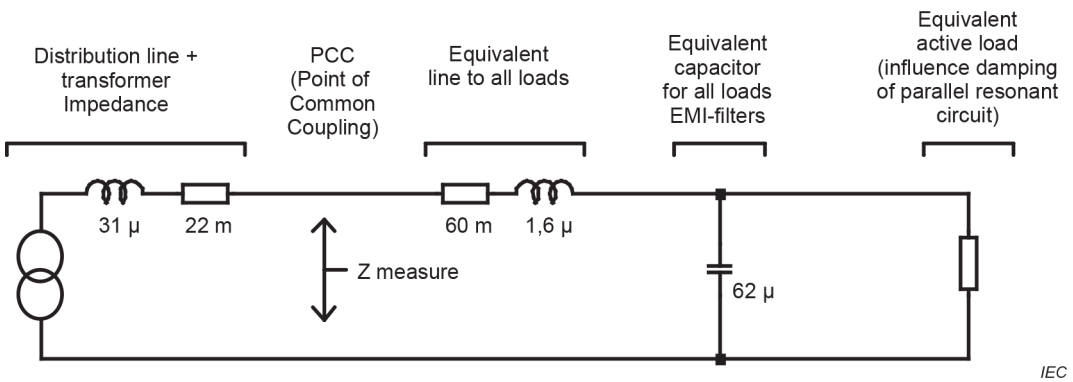

Figure 13 – Resulting simplified model of the charging hub with distribution lines and feeder

The connected charging stations and photovoltaic system only slightly influence the grid impedance in the frequency range from 50 Hz to 2 450 Hz. This can be explained by the very short connection to the local transformer station (about 80 m away), the high-power rating of the transformer (1 MVA) and its low short-circuit voltage (U_k = 4,6 %). The influence of the transformer on the FdGI is in this case dominant in comparison to the individual consumers.

Documents
Document Sharing Hub

In the lower frequency range (150 Hz to 2 kHz) and in the upper high frequency range (50 kHz to 150 kHz), the FdGI is mainly shaped by the supply line to the transformer and by the outgoing feeders to the loads, respectively. In the frequency range from 2 kHz to 50 kHz, resonances can be recognized (see Figure 14). The series resonance at about 16 kHz is due to the inductances of the feeders to the connected loads with the EMC filters. The parallel resonance at about 3,5 kHz is due to the supply line of the transformer station in connection with the same EMC filter capacitors.

Figure 12 confirms the assumption that the low frequency range is influenced by the short-circuit power of the transformer, while the high frequency range is influenced by the EMC filters of all devices connected to the main busbar. Thanks to the absence of residual current protections, larger devices such as chargers and PV inverters with large C_x and C_y capacitors are likely to have even more influence than smaller household appliances (especially multimedia and computers). Small household appliances can affect the impedance with possible resonance from 150 kHz onward, due to smaller C_x and C_y capacitors in their EMC filters. However, in the case of the connection of hundreds of such devices, the resulting capacitance is considerably larger, thus shifting possible resonances to much lower frequency ranges.

The larger active loads connected to the busbar (e.g. fast charging stations) are damping the parallel resonance in the lower frequency range. The impact of a super-fast EV charger is presented in Figure 14 as an example:

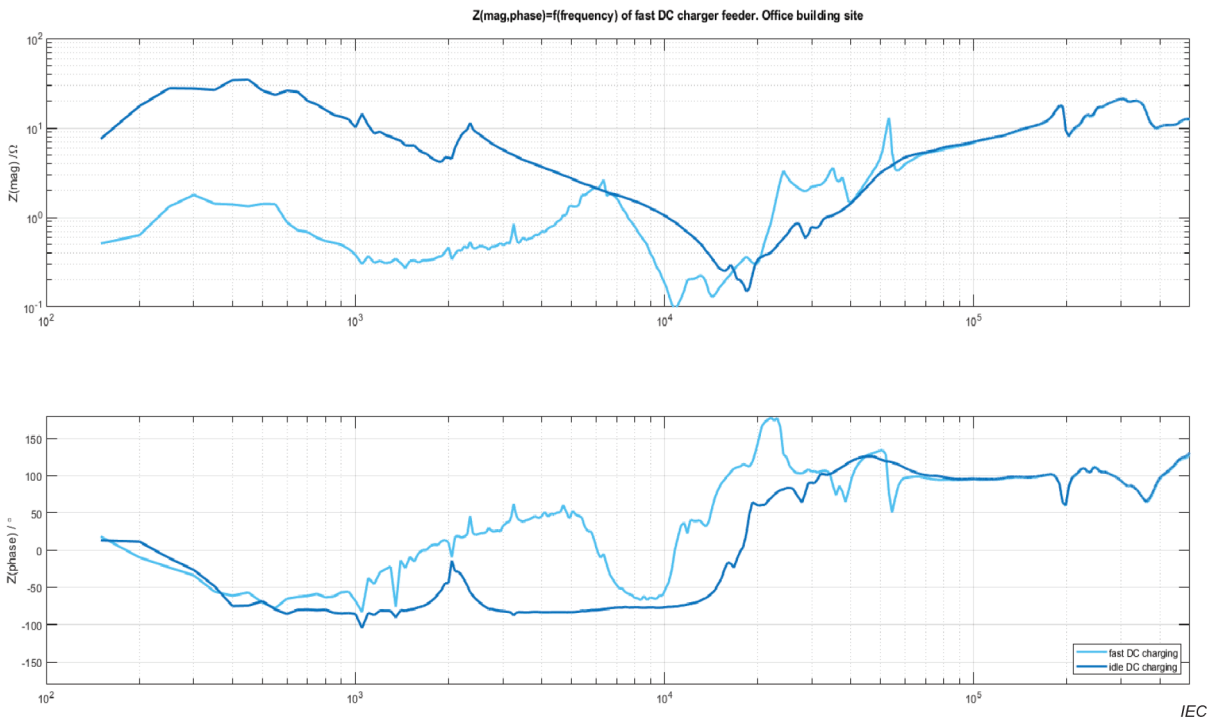

Figure 14 – Impact of a super-fast EV charger on grid impedance

The analysis of Figure 12 leads to the following conclusion: The current harmonics generated by an inverter by PWM modulation hardly flow to the transformer when the transformer station is relatively far away, because the impedance to the transformer station is much higher than the impedance to other devices connected to the same busbar.

Documents
Document Sharing Hub
Full document details: PD IEC TR 61000-2-15:2023

Even though conducted emissions are very low at that frequency, current distribution between loads and sources can be predicted and verified at 8,1 kHz, where both the current harmonics and power line impedance of the individual feeders are measured. At that frequency, small current emissions can be traced with long-term measurements back to one of the inverters. The impedance and current running through the feeders are displayed in Table 1. The current drawn from the PV system at 8,1 kHz runs into the feeder with the lowest impedance. Since the measurements in the feeders are performed one after the other, the sum of the currents of all feeders deviates slightly from the total current of the PV system. Figure 14 shows that the current drawn by the PV inverter mainly flows into the offices and workshops, i.e. where the impedance is lowest at 8,1 kHz. As described in Clause 4, the phase angle of currents and impedances can be considered for more accurate analysis.

Table 1 – Relation between measured current and respective impedance for each feeder

Feeder	Impedance, Z_h at 8,1 kHz, in Ω	Measured current at 8,1 kHz in mA
PV-installation (source for the emission)	-	29
Fast EV charger (no charging car)	1,51	5,9
On-board chargers	2,69	6,8
Feeder from transformer station	1,55 (estimated from the model)	7,1
Office and workshop facilities	0,41	28

In conclusion, a simplified circuit model of the installations, including the transformer, lines EMC filters and power converters can be obtained on the basis of FdGI measurements. Computer simulations in the frequency domain analysis can help predict resonances and excessive current flowing from one converter to the other as described in 4.1.1. A standardized indication of converter input capacitance and switching frequency can make a preliminary assessment about compatibility between a new converter and an existing grid section.

4.3 Impact of power electronic household equipment on the impedance characteristics in residential networks

The input impedance of power electronic (PE) equipment often has capacitive characteristics [5],[7]. Large amounts of such equipment (i.e. in households or office buildings) can consequently introduce a significant capacitance into the public low voltage networks, which can form a resonance with the inductances of the lines and the supply transformer. To study this impact, different combinations of typical household devices, which are further referred to as load scenarios, have been defined. For each load scenario, the input impedance characteristic up to 2 kHz has been measured using the method described in [6], [8] Based on the measured impedances, a suitable equivalent (impedance) circuit model is introduced, and its parameters are identified based on a vector-fitting approach. The equivalent models for the load scenarios are finally integrated into a residential LV network simulation model and different evolution stages of PE penetration, namely past, present, and future have been simulated [5], [6].

Documents
Document Sharing Hub
Full document details: PD IEC TR 61000-2-15:2023

The device topologies in the load scenarios vary according to the evolution stages as shown in Table 2. Lighting loads (D3 to D5) have been transformed from incandescent lamps in the past to CFLs (compact florescent lamps) and LEDs (light-emitting diodes) at present, and exclusively LEDs in the future. A similar transition can be considered for refrigerators and vacuum cleaners, which have evolved from simple capacitive-start induction-run motor devices to devices with PE front-ends including active power factor correction (aPFC) over the last few decades. The three distinct evolution stages are considered to elucidate the increased proliferation and replacement of several passive loads by PE-based loads for most common household devices as per [9] In the "past", the share of passive loads was higher, and the only PE-based loads were computers (PCs) and televisions (TVs). The PE-based devices in all load scenarios can be categorized into non-power factor corrected (nPFC), passive-power factor corrected (pPFC), and active-power factor corrected (aPFC) circuit topologies.

Table 2 – Devices and topologies used in the different evolution stages

Device (D)	Device name	Past (A)	Present (B)	Future (C)
1	Refrigerator	Passive	Passive/aPFC	aPFC
2	Router	N/A	nPFC	nPFC
3	Incandescent lamps	Passive	N/A	N/A
4	CFL	N/A	nPFC	N/A
5	LED	N/A	nPFC/aPFC	nPFC/aPFC
6	PC	n-pfc	pPFC/aPFC	aPFC
7	Laptop	N/A	nPFC	nPFC
8	Hotplate/ Water cooker	Passive	Passive	Passive
9	Induction stove	N/A	aPFC	aPFC
10	TV	nPFC	nPFC/aPFC	aPFC
11	Hair dryer	Passive	Passive	Passive
12	Vacuum cleaner	Passive	Passive/nPFC	nPFC

The methodology proposed in [9] is used to identify the set of devices connected at a given time instance of the day. In this study, three different time instances in a day depending on the power demand at the fundamental frequency are considered, namely peak demand (evening), average demand (morning and afternoon) and low demand (after midnight). In combination with the three different evolution stages past (A), present (B) and future (C), this results in a total of nine load scenarios (IA, IB, IC, IIA, ...), as shown in Table 3 for which the individual sets of devices are given. In all the device sets, passive devices, which transition into PE-based devices, are equi-proportionately replaced across various evolution stages.

Table 3 – Load scenarios depending on the evolution stages and loading conditions

	Set of devices		
Evolution stage (*k*)	**I (low demand)**	**II (average demand)**	**III (peak demand)**
Past (A)	$D_{A1}+D_{A3}$	$D_{A1}+D_{A3}+D_{A6}$	$D_{A1}+D_{A3}+D_{A6}+D_{A8}$
Present (B)	$D_{B1}+D_{B2}+D_{B4}+D_{B5}$	$D_{B1}+D_{B2}+D_{B4}+D_{B5}+D_{B6}$	$D_{B1}+D_{B2}+D_{B4}+D_{B5}+D_{B6}+D+D_{B9}$
Future (C)	$D_{C1}+D_{C2}+D_{C5}$	$D_{C1}+D_{C2}+D_{C5}+D_{C6}$	$D_{C1}+D_{C2}+D_{C5}+D_{C6}+D_{C9}$

The measured frequency-dependent input impedance of each load scenario has been fitted into an RL||RLC equivalent circuit. Table 4 provides the equivalent parameters for all nine-load scenarios.

AVA Documents
Document Sharing Hub
Full document details: PD IEC TR 61000-2-15:2023

Table 4 – Equivalent $R_{L1}L_1||R_{L2}L_2C_2$ parameter values

Scenario #	R_{L1} (Ω)	L_1 (mH)	R_{L2} (Ω)	L_2 (mH)	C_2 (μF)
IA	340	0	0	0	0
IB	400	0	30	0	4,5
IC	230	0	40	0	3,1
IIA	30	0	28	1	7,5
IIB	100	0	20	0	7,5
IIC	50	0	15	0,6	15
IIIA	28	0	28	0	10
IIIB	36	8,83	9,5	6,33	12,3
IIIC	50	0	14	0	12

The equivalent load models and the corresponding parameters derived are implemented in an urban residential LV network (single-fed, radial structure). The urban network supplies 180 households with a 630 kVA MV/LV-transformer. The respective load scenarios are applied to all customers representing an “average device scenario” although in practical cases the load scenarios most likely differ between different customers even at one considered time instant (i.e. peak load). This distribution of various load scenarios amongst various households is considered as a scope of future work.

Figure 15 shows the magnitude and the phase angle of network harmonic impedances simulated at the LV busbar of the MV/LV transformer $\underline{Z}_{\mathrm{B\,Dk}}$ and the customer-side harmonic impedances $\underline{Z}_{\mathrm{C\,Dk}}$ (part of the network impedance representing all impedances downstream the LV busbar) for the nine load scenarios. The presence of a resonance can be identified, if the simulated magnitude of the nodal impedance curve for the load scenario is above the impedance line $\underline{Z}_{\mathrm{B\,ext}}$ extrapolated based on the impedance at fundamental frequency. The resonance does not exist for all “past” scenarios. This can be attributed to the lower capacitances or absence of capacitances and higher damping provided by the passive devices in the respective load scenarios (IA, IIA, IIIA) as shown in Figure 15 (c) and (d). As the number of PE-based devices increases and the number of passive devices decreases, the possibility of resonance increases for the present and future evolution stage. It can be seen from Figure 15 (c) and (d), that the customer-side phase angles are decreasingly capacitive for “present” and “future” evolution stages.

Documents
Document Sharing Hub
Full document details: PD IEC TR 61000-2-15:2023

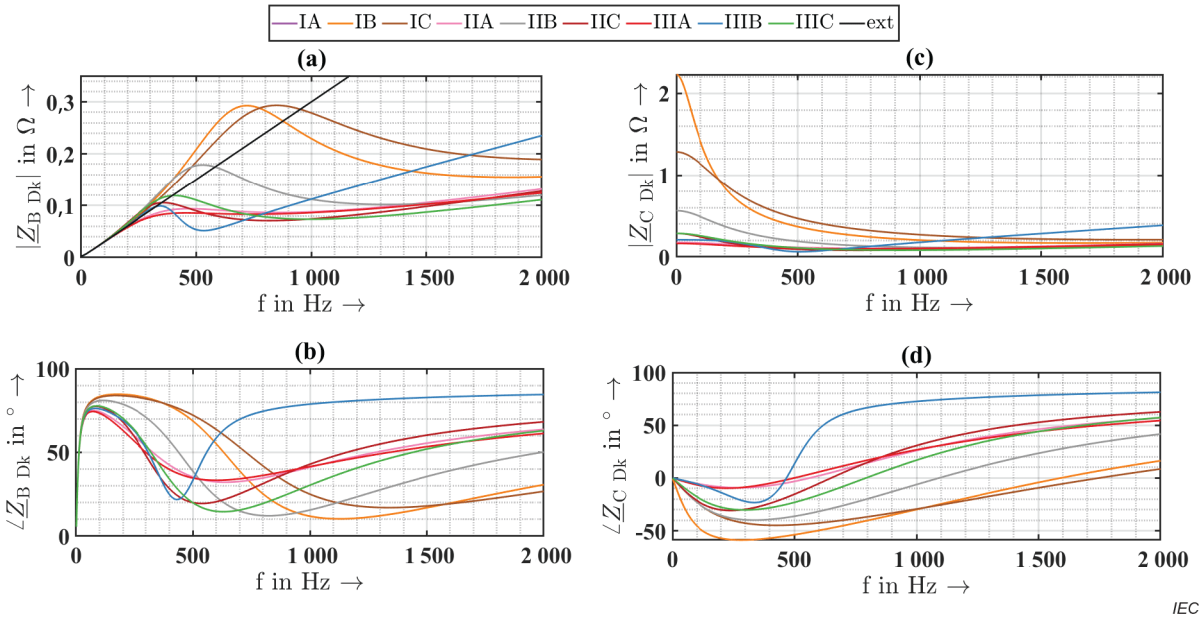

Busbar: (a) magnitude, (b) phase angle; customer-side: (c) magnitude, (d) phase angle.

Figure 15 – Impedance characteristics of an urban LV network,

The intensity of the resonances is characterized by the magnitude ratio ($k_{\text{A Dk}}$) between the network harmonic impedance and the extrapolated impedance based on the value at the fundamental frequency. Table 5 shows the resonance frequency and the magnitude of the ratio ($k_{\text{A Dk}}$) for the nine scenarios.

Table 5 – Ratio between network harmonic impedance and extrapolated impedance for various cases

Scenario #	f_r (Hz)	$k_{\text{A Dk}}$	Scenario #	f_r (Hz)	$k_{\text{A Dk}}$	Scenario #	f_r (Hz)	$k_{\text{A Dk}}$
IA	N/A	N/A	IIA	N/A	N/A	IIIA	N/A	N
IB	608	1,47	IIB	412	1,27	IIIB	N/A	N/A
IC	656	13	IIC	251	1,15	IIIC	284	1,15

In case of low power demand (device set I), in the future, this can lead to higher resonance frequency and lower value of $k_{\text{A Dk}}$ due to lower capacitive and higher resistive characteristics of the customer-side impedance compared to the "present" (see Figure 15 (d)). It can be seen from Table 5 for low load demand (scenarios Ik) and average load demand (scenarios IIk), that the resonance frequency and the ratio $k_{\text{A Dk}}$ decrease in the "future" compared to the "present" due to higher capacitive and higher resistive characteristics of the customer-side impedance.

For the peak load demand (scenarios IIIk), the urban network does not possess any resonance characteristics for the "present" and only a less pronounced resonance in the "future". Based on the results, it can be inferred that despite higher equivalent capacitance for individual customer the value of $k_{\text{A Dk}}$. does not necessarily increase, but the resonance frequency tends to be reduced.

Documents
Document Sharing Hub
Full document details: PD IEC TR 61000-2-15:2023

It can be further concluded that the PE-based devices increase the probability of harmonic resonance in the “present” and “future” with varied intensity levels depending on the evolution stages and load demand. The amplification level and the resonance frequency of resonances in the future are expected to be lower compared to the present situation. Further details on this study can be found in [10].

4.4 Harmonic resonance in an urban, residential low voltage grid

The LV network considered in this case study is located in a major city in Germany and its layout is presented in Figure 16. It supplies about 240 domestic customers in single-family houses and apartment houses as well as 85 streetlights. No shunt capacitor banks are connected to the network.

Each streetlight contains a grid-side shunt capacitance for power factor correction at power frequency and behaves as strongly capacitive at frequencies higher than 100 Hz. The network is operated as a meshed grid and has a high short circuit power (about 3 MVA at the three junction boxes).

The network has been built about 10 years ago on “greenfield”. Usually in such strong, newly built networks, no power quality problems are expected. This suggests that most of the domestic customers have a dominating share of modern energy-efficient power electronics, which also introduces a significant amount of shunt capacitance.

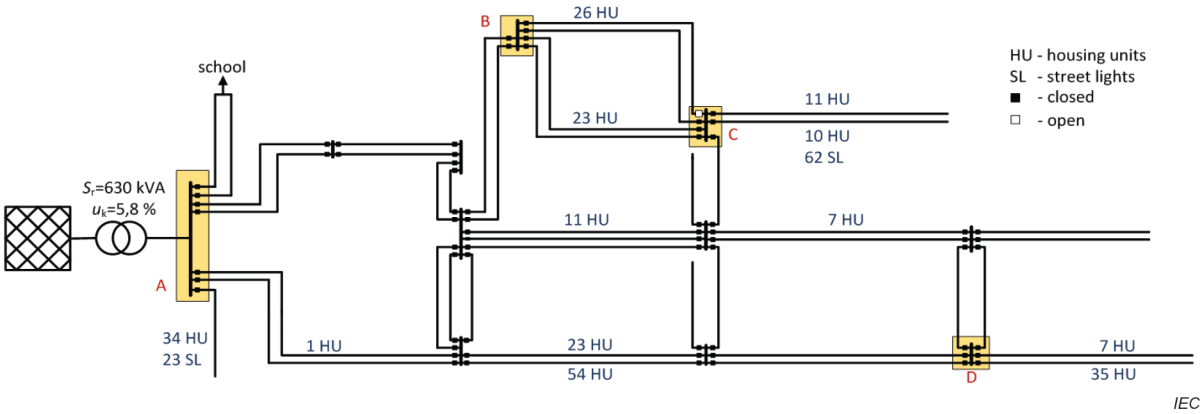

Figure 16 – Schema of the network

Routine measurements by the distribution system operator (DSO) indicated the existence of a resonance around 500 Hz. In particular, a strong amplification of mains signaling voltage by a factor of 2,5 and sudden, significant changes in harmonic levels in case of switching the streetlights have been observed.

The network harmonic impedance has been measured at the junction boxes (B, C, and D in Figure 16) and the LV busbar (A in Figure 16). Figure 17 presents an example of magnitude and phase angle of the network harmonic impedance L1-N measured at a time instant during the day, when the streetlights are switched off.

Documents
Document Sharing Hub
Full document details: PD IEC TR 61000-2-15:2023

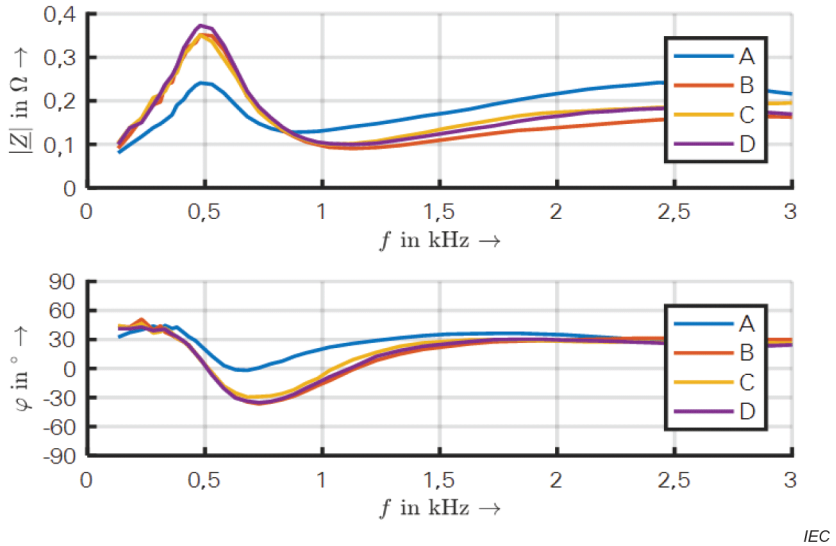

Figure 17 – Network harmonic impedance measured at different locations (L1-N)

Loop impedances L2-N and L3-N are similar, and no significant variations have been observed at different times of the day. At all locations A to D, a pronounced parallel resonance around 500 Hz is observed. As the frequency used for mains signaling is, with 482 Hz, very close to the resonance frequency, it is confirmed that the aforementioned amplification of mains signaling levels in this network is caused by the resonance. As streetlights are switched off during the day and line capacitances in LV networks are too small to cause resonances at such low frequencies, the only reason for the resonance can be the distributed capacitance of the domestic customers.

To study the reasons for the resonance, a detailed simulation of the network has been developed. At first, the network harmonic impedance at the locations A to D has been simulated using default elements, which means π-equivalence for lines, series R-L equivalence for MV/LV transformers and parallel R-L equivalence for the domestic customers. The results without streetlights are presented in Figure 18 and do not show any resonance. This confirms that line capacitances cannot be the reason for the measured resonance.

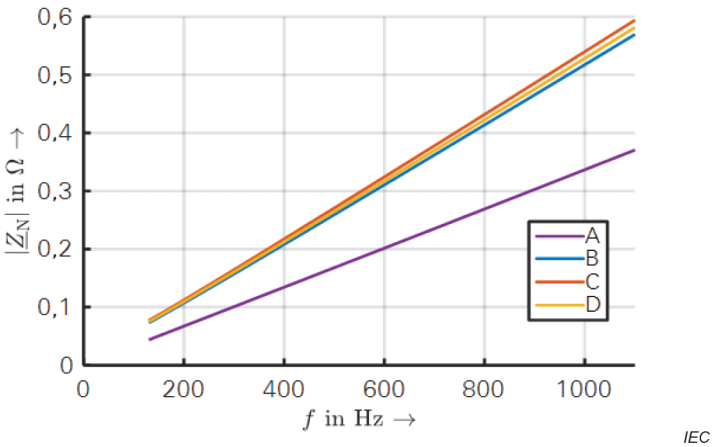

Figure 18 – Simulated network harmonic impedance at different locations (L1-N) using default element representations

In a second step, a suitable equivalent circuit has been developed and parameterized for the domestic customers to match the measured impedances as closely as possible (see Figure 19).

AVA Documents
Document Sharing Hub
Full document details: PD IEC TR 61000-2-15:2023

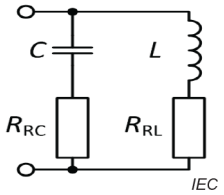

$C \approx 5$ µF; $R_{RC} \approx 0{,}5$ Ω;
$L \approx 95$ mH; $R_{RL} \approx 130$ Ω

Figure 19 – Equivalent impedance model of a domestic customer

The results are presented in Figure 20. They show a good match with the measurements (dots) for the three junction boxes, while at the LV busbar the simulation is slightly too low. It can be noted that the model is a specific harmonic load model providing satisfying results at frequencies around the first resonance but is not suitable for simulations at power frequency.

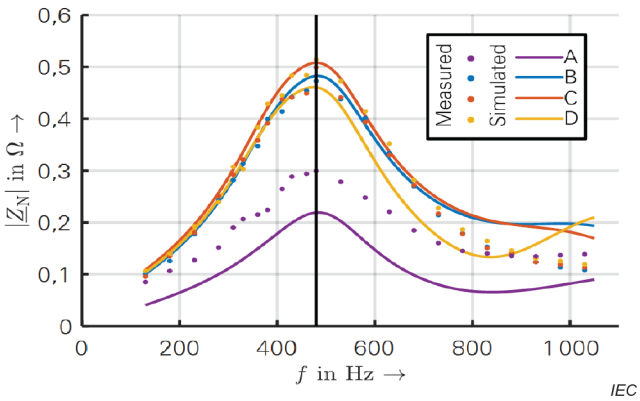

Figure 20 – Measured and simulated network harmonic impedance at different locations (L1-N) using the developed customer impedance model

The streetlights have only a minor impact on the resonance. If they are switched on during the night, the resonance shifts to slightly lower frequencies, because slightly more capacitance is connected to the grid.

The case study shows that modern power electronic converters can cause significant resonances at low harmonics in residential LV networks. Besides amplification of harmonic voltages and currents, this can also lead to harmonic instabilities together with for example PV-inverters or converters for battery storage. As these capacitances are distributed in the network, detuning as in the case of dedicated capacitor banks is not an option. In the case where resonance causes harmonic voltages above the compatibility levels (e.g. in accordance with IEC 61000-2-2 [64]), the most promising option is an impedance shaping by active filters. The presented study has clearly shown that harmonic resonances in LV networks cannot be neglected anymore. DSOs may consider including such issues already in the process of network planning. Further, resonances can also be considered when calculating harmonic emission limits for customer installations.

Further details on the presented study can be found in [5].

Documents
Document Sharing Hub
Full document details: PD IEC TR 61000-2-15:2023

4.5 Harmonic distortion and impedance characteristics in an islanded microgrid

The frequency-dependent grid impedance (FdGI) forms the link between voltage and current distortion and is one of the key parameters for managing electromagnetic compatibility (EMC). In 100 % power electronic–based networks, the FdGI is expected to be considerably different compared to “traditional” interconnected grids, which might have a considerable impact on future EMC coordination strategies, especially the definition of emission limits.

In order to study the impact of the supply grid configuration on the FdGI as well as voltage and current harmonics, the laboratory setup presented in Figure 21 is used.

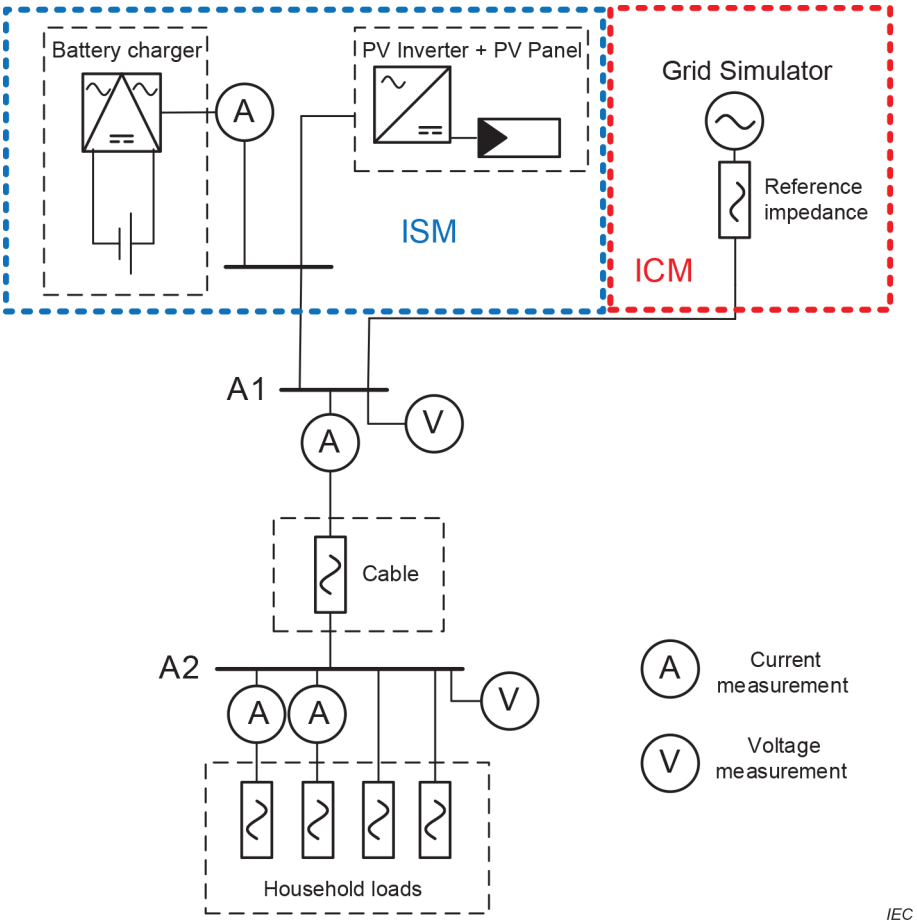

Blue box: islanded mode; red box: interconnected mode.

Figure 21 – Schematic representation of system under test

The system can operate in the islanded mode (ISM; blue dashed box) and interconnected mode (ICM; red dashed box). In ISM, the source is a combination of a battery-fed voltage-controlled converter and a PV inverter, which synchronizes to it and operates in current-controlled mode. In ICM, the source comprises a grid simulator and a reference impedance as defined in IEC 61000-4-7:2002/AMD1:2008, [65] Annex B. Various types of loads as summarized in Table 6 are connected.

Documents
Document Sharing Hub
Full document details: PD IEC TR 61000-2-15:2023

Table 6 – Load scenarios

Scenario	Load type	Total power demand
Load 1 (L1)	Non-power factor corrected (nPFC)	715 VA
Load 3 (L3)	Active power factor corrected (aPFC)	390 VA
Load 4 (L4)	Passive	4 000 VA
Mixload (MI)	nPFC+aPFC+passive	4 600 VA

The loads are classified as non-power factor corrected (nPFC), active power factor corrected (aPFC), and passive. The nPFC loads (L1) are composed of a variety of lamps such as CFL and LED. The aPFC loads (L3) are composed of a laptop charger and several PC loads. Passive loads (L4) are water cookers and incandescent lamps. The mixload scenario (MI) is obtained by a combination of a variety of the above-mentioned loads.

For each of the scenarios, measurements of the FdGI (see Figure 22) as well as voltage and current harmonics in the frequency range up to 2 kHz have been carried out at the busbar A1. The network impedance in Figure 22 (e) and (f) is determined as a parallel circuit of the upstream and downstream impedance at busbar A1. The upstream impedance corresponds to the grid-side impedance in Figure 22 (a) and (b) and the downstream part to the load-side impedance in Figure 22 (c) and (d). The presentation and discussion of results is limited to those scenarios involving power electronic loads (L1, L3, and MI).

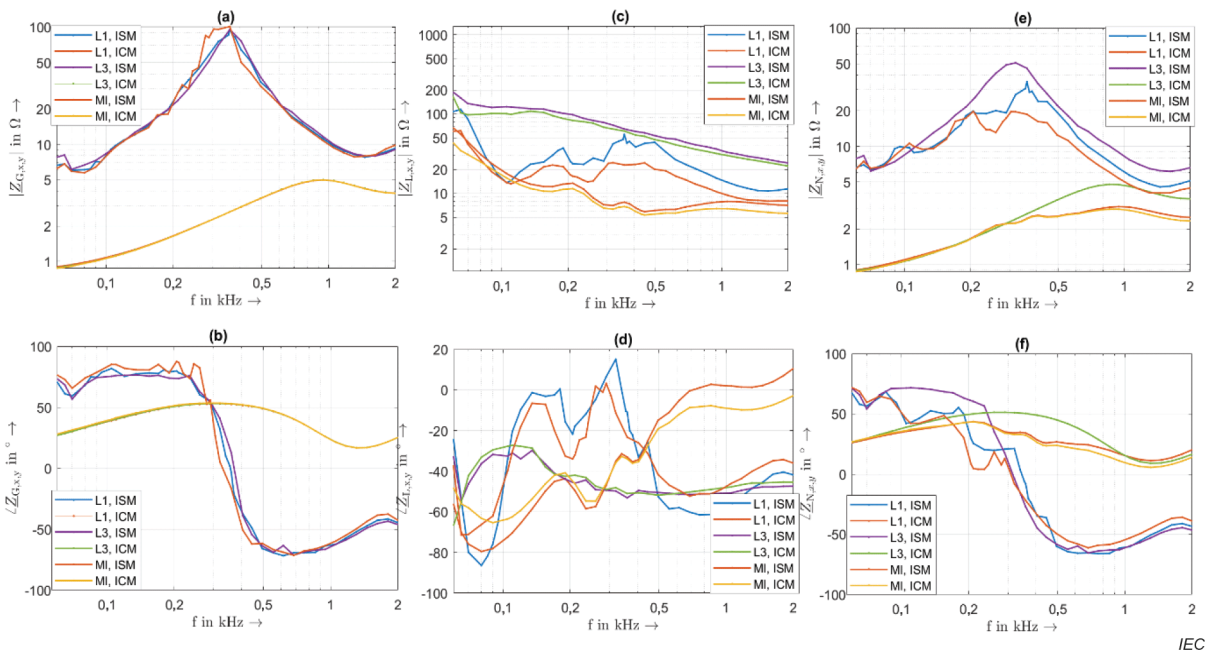

Grid-side and upstream impedance (a), (b); load-side and downstream impedance (c), (d); and network and total impedance (e), (f).

Figure 22 – Impedance characteristics (magnitude and phase angle)

The grid-side impedances as shown in Figure 22 (a) and (b) are far lower in magnitude for ICM compared to ISM. Both are virtually independent of the load scenario. The magnitude of short-circuit impedance for ISM is about 5,8 times higher than in ICM. In ISM, the grid comprises a strong resonance at around 350 Hz (7th harmonic) where the impedance is about 33 times higher than in ICM.

Documents
Document Sharing Hub
Full document details: PD IEC TR 61000-2-15:2023

The origin of the resonance can be attributed to the grid-side filter circuits and closed-loop controllers in the respective sources (battery and PV) and the interaction between them. The phase angle characteristics in ICM remain resistive-inductive in the considered frequency range, while they get highly capacitive in ISM beyond the resonance frequency. Figure 22 (c) and (d) shows the load-side impedance characteristics. All presented scenarios exhibit capacitive behaviour in large ranges, which is caused by the character of the power electronic devices. As expected, the operation mode of the grid has no significant impact on their behaviour.

Figure 22 (e) and (f) presents the network impedance characteristics of ICM and ISM. While in ICM for scenario L3, due to the rather high load-side impedance, the network impedance is virtually like the grid-side impedance, for scenarios L1 and MI a visible influence at frequencies above 250 Hz can be observed. In case of ISM, although the resonance frequency remains unaffected, the resonance magnitude is reduced for the three load scenarios with the smallest reduction for scenario L3. The phase characteristics are comparable between the grid-side and network impedances for all load scenario and both operating modes. As for grid-side impedances, the magnitude of the network impedance is far higher for ISM compared to ICM.

Figure 23 presents the voltage harmonic levels for both operation modes. In ICM, the harmonic voltages are almost independent of the load scenario and are determined by the background distortion that has been set in the grid simulator in order to represent a voltage distortion typically found in residential LV networks. In ISM, the background voltage without any load connected is much lower compared to ICM, but the load scenarios have a considerable impact on the voltage harmonic levels. A favorable cancellation exists between the different devices in scenario MI, which in turn results in the lowest harmonic voltage levels.

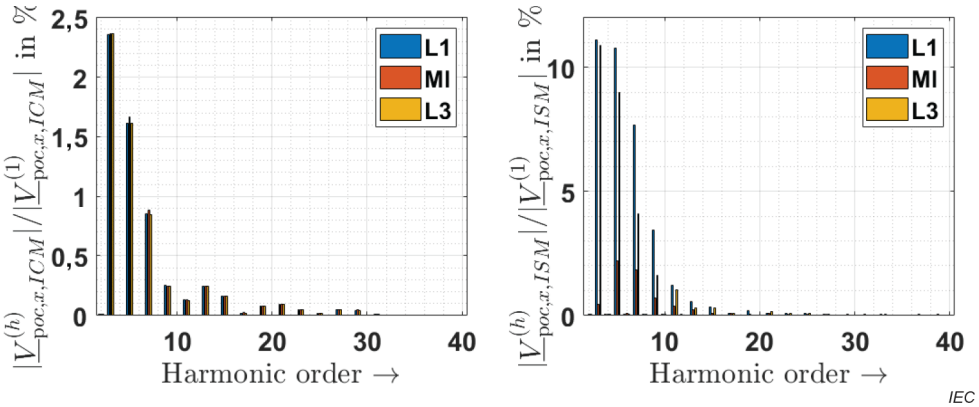

Figure 23 – Voltage harmonic levels in ICM (a) and ISM (b)

The experimental results prove that due to the higher network impedance in ISM the voltage harmonics are significantly amplified compared to ICM. The impact of background voltage is higher in case of ICM. It can be concluded that the generation of voltage distortion by the respective distorting loads is qualitatively different between ICM and ISM. Moreover, in ISM pronounced resonances will be expected in the FdGI. These results confirm that the harmonic characteristic in 100 % power electronic–based grids, particularly the smaller ones, differs considerably from the present conditions in interconnected networks. This may be considered in future EMC standardization. Further details and measurement results can be found in [6]

Documents
Document Sharing Hub
Full document details: PD IEC TR 61000-2-15:2023

5 Impact of modern power electronics on the propagation and amplification of voltage distortion

5.1 Harmonic propagation in a residential LV network

5.1.1 General

In the following, the case is illustrated of a residential area where significant voltage amplitude variations of the 15th harmonic were registered. The issue was due to the operation of large heat pumps connected to the grid.

Furthermore, the voltage level at each grid point is not only influenced by the operation of such inverters, but higher harmonic voltage amplitudes can be expected, caused by the sum of all loads in the grid [27]

Figure 24 represents the single line diagram of a residential area hosting a building complex where the heat is generated by two heat pumps: a large one powered by a 150 kW inverter and a small heat pump driven by a 35 kW inverter. The grid is analyzed in the PowerFactory[2] software [28], see below:

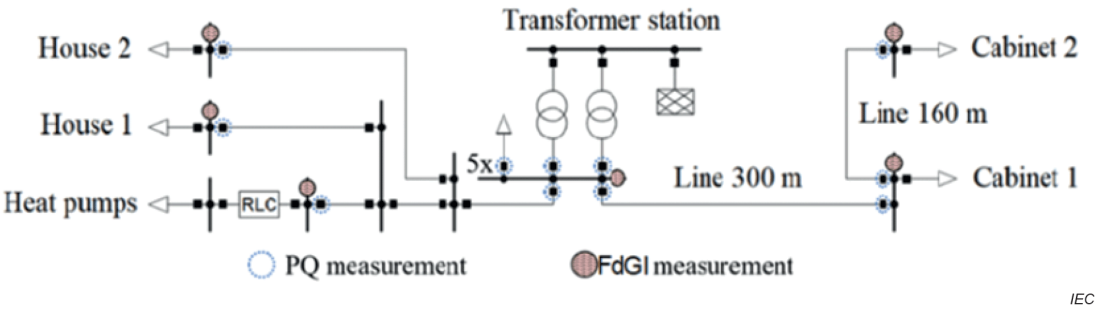

Figure 24 – Simplified line diagram of the grid with marked measuring points

5.1.2 Measurements

In two measurement campaigns, 6 grid nodes were monitored with 15 PQ measuring devices (PQ-Box 100/150/200, a-eberle). Additionally, the FdGI was measured and analyzed. The transformer stations, house 1 and house 2, belong to the building complex where the heat pumps are installed. The remote cabinets 1 and 2 are connected to the transformer station by long cables of 300 m and 160 m. In the standard situation, there was no active filter (corresponding to the node RLC in Figure 24) installed.

To measure PQ parameters, voltage sensors were connected to the three phases L1 to L3, to neutral N and to protective earth PE (see Figure 25), corresponding to measurement category CAT IV. The terminals of voltage probes connected to the feeders are equipped with fuses. The current sensing was performed by Rogowski coils or current clamps. The neutral conductor current was measured. Measurement data were saved as RMS values in 1 min intervals with Class A devices in accordance with IEC 61000-4-30 [66] to achieve sufficient accuracy.

[2] PowerFactory is the trade name of a product supplied by DIgSILENT GmbH. This information is given for the convenience of users of this document and does not constitute an endorsement by IEC of the product named. Equivalent products may be used if they can be shown to lead to the same results.

AVA Documents Document Sharing Hub